# Analysis of self-pulsing in absorptive optical bistability

M. Gronchi,* V. Benza, and L. A. Lugiato
*Instituto di Fisica dell'Universita, Via Celoria 16, 20133 Milano, Italy*

P. Meystre
*Max-Planck-Institut für Quantenoptik, D-8046 Garching, Federal Republic of Germany*

M. Sargent III
*Optical Sciences Center, University of Arizona, Tucson, Arizona 85721*

(Received 27 October 1980)

We review and extend the theory of instabilities in absorptive optical bistability for ring cavities containing homogeneously broadened two-level media. The instabilities occur in the high-transmission branch and result in either a precipitation to the low-transmission branch or in pulsed multimode operation. Two numerical approaches are used to predict operation away from the simple mean-field limit. First, an iterative method is used to solve the general field eigenvalue equation for cavity modes with frequencies displaced from the input frequency. This work shows that the instability region decreases in size as the mirror transmission increases. These calculations are confirmed by the second numerical technique, consisting of direct integrations of the coupled Maxwell-Bloch equations. This second approach also provides time histories of the instability evolutions, and divides the instability range into a precipitation regime and a self-pulsing regime. The results are discussed in terms of first- and second-order phase transitions, and agree with the analytical results obtained within the dressed-mode description of optical bistability. They show that when the incident field is adiabatically decreased along the high-transmission branch, the spiking behavior always appears abruptly. By further decreasing the incident intensity, the self-pulsing disappears either continuously if the system remains in the high-transmission branch, or discontinuously if the system precipitates to the low-transmission branch. Connection is made with induced probe gain known in the saturation spectroscopy of absorbers (uninverted media), in which population pulsations transfer energy from a saturating wave to the probe waves. The very close relationship with multimode operation in homogeneously broadened unidirectional ring lasers is also established.

## I. INTRODUCTION

Some recent papers[1-4] have developed the exact semiclassical treatment of absorptive optical bistability[5] for two-level systems in a ring cavity. In this problem, a cw input field of suitable amplitude is tuned to the atomic line center and to a cavity eigenfrequency, and leads to a transmitted field having three possible amplitudes, two of which are stable. The larger stable amplitude corresponds to bleaching of the saturable absorber, the smaller to nearly linear absorption. The analysis of Refs. 1–4 takes propagation effects into account, that is, the internal-field amplitude can vary along the cavity axis. The main result of these papers is that appropriately intense input fields produce instabilities in the high-transmission branch. Specifically in contrast to the cw input field, the transmitted field can show a time-varying, pulsing behavior.[3] This suggests that the bistable absorber could be used to convert cw light into pulsed light. The stability analysis of Refs. 2 and 3 uses the Maxwell-Bloch equations to study the possible buildup of field modes other than the principal centrally tuned one. Explicit instability conditions were obtained subject to two assumptions: (1) only the centrally tuned modes could saturate the medium, and (2) the "mean-field limit" is valid, that is,

$$\alpha L \ll 1, \quad T \ll 1, \tag{1}$$

with $C = \alpha L/2T$ constant, where $T$ is the mirror transmittivity, $\alpha$ is the linear absorption coefficient, and $L$ is the length of the absorber. The instability conditions showed that modes close to detuned cavity eigenfrequencies could build up.

In limit (1), the dynamics of the system are governed by the *modes* of the cavity. In particular, the mode that is resonant with the incident field plays a dominant role. Under ordinary conditions and apart possibly from initial transients of duration on the order of the cavity buildup time, the electric field, as well as the polarization and inversion fields, are practically uniform in space.[1,6] Optical bistability is then correctly described by the mean-field theory, in which propagation effects are neglected and only the resonant mode is considered.[7,8]

The instabilities in absorptive optical bistability can be expressed in terms of the differential gain $G$:

$$G = -\alpha L \frac{dV}{dE_T} .$$

 

Here $V$ is the dimensionless induced polarization in quadrature with the field ($V$ of the Bloch vector $U$, $V$, and $W$ components), and $E_T$ is the transmitted electric-field amplitude. For stability, the losses must exceed this gain, i.e.,

$$1+2C\frac{dV}{dE_T}>0\,.$$

Comparison with the state equation[1]

$$E_I=E_T+2CV\,,$$

where $E_I$ is the input-field amplitude, reveals that the stability condition is the same as that for a positive slope $dE_I/dE_T$. Instability results for a negative slope.

References 2 and 3 have shown that under special conditions still satisfying (1), the off-resonant modes of the cavity may play an important role. This occurs whenever at least one of them sees gain, that is, the $-dV/dE_T$ at that side-mode frequency exceeds the corresponding losses. Hence as for the single-mode instability described above, this multimode instability corresponds to a negative slope of $E_I$ vs $E_T$, but evaluated at the side-mode frequency. The steady state is then unstable and the system begins to emit pulses.[3] Under suitable conditions, this sequence of pulses becomes periodic and of infinite duration. This undamped spiking behavior is called "self-pulsing" because it is not the consequence of an external manipulation, but rather is spontaneously induced by the self-organization of the system.[9] In the self-pulsing regime, the purely passive optical-bistable system works as a novel type of laser without population inversion. The nonlinear atom-field interaction transfers energy from the incident light to the side modes, and the cavity feedback allows these modes to grow, leading to the spiking behavior. This is closely related to the multimode operation that occurs in the homogeneously broadened unidirectional ring laser beyond the second threshold.[10,11] From a practical viewpoint, the present system provides an all-optical device capable of transforming cw light into pulsed light. Such a transformation has been predicted and observed by McCall[12] using a hybrid system that feeds part of the transmitted light back into the cavity via a nonlinear electro-optical device. The physics of McCall's device is quite different from that considered here. Another instability discussed by Ikeda[13,14] and seen in a hybrid system by Gibbs *et al.*[15] occurs when the differential equation eigenvalues are negative, but the difference equation defining the boundary conditions is nevertheless unstable. Ikeda did not predict this kind of instability to occur in the purely absorptive-bistability case considered in the present paper, but the subject remains one of active research. In particular, it is interesting to note that a multimode gain instability with more than three modes could have a quasi-periodic character with some chaotic behavior much like that of a five-mode nonmode-locked, i.e., free-running, laser.

The present paper reviews the basic theory[1-4] and discusses the results of two kinds of numerical calculations that illustrate the range and nature of the instability. First we solve the field eigenvalues of Ref. 2 numerically, allowing the centrally tuned mode amplitude to vary in space. We show that the range of instability (versus input field) decreases as $T$ and $\alpha L$ increase, and ultimately disappears altogether. The largest instability occurs in the mean-field limit. However, we note that the range of the bistability itself decreases as $T$ increases, and our data reveal that the ratio of the instability range to the bistability range increases as $T$ increases. Secondly we integrate the coupled Maxwell-Bloch equations to observe the time development of the instability for various combinations of parameters. These numerical integrations yield the same instability regimes as those from the eigenvalue analysis. In addition, they allow us to explore the nonlinearities that lead to self-pulsing or precipitation. In particular, we show that the transition from steady state to self-pulsing is of first order on the "lower" boundary of the instability region and of second order on the "upper" boundary. This has been confirmed analytically in the framework of a dressed-mode theory.[16-18] In practice, this means that if we decrease the incident intensity along the high-transmission branch, the self-pulsing always appears abruptly. By further decreasing the incident intensity, the self-pulsing disappears continuously or discontinuously according to whether the system remains in the high-transmission branch or precipitates to the lower-transmission branch. We have determined numerically the parts of the instability region leading to self-pulsing and to precipitation. Although chaotic behavior[13] is possible in principle, we have not found any evidence of it in our model.

This paper is organized as follows. In Sec. II, we review the Maxwell-Bloch equations used to describe the atom-field interaction with boundary conditions appropriate for a ring cavity. The main features of the steady-state solutions[1] are recalled. The linear stability analysis of the stationary solutions is performed in Sec. III. As shown in Ref. 2, this analysis leads to an exact eigenvalue equation. In order to give a self-contained description of self-pulsing, the explicit

mean-field solution[3] is reviewed in Sec. IV. Section V discusses properties of the eigenvalues in the mean-field limit that do not remain valid in the general case. The results of the numerical integration of the exact eigenvalue equation are given in Sec. VI. The results of the Maxwell-Bloch integrations are presented in Sec. VII, showing the exact instability region, the self-pulsing and precipitation domains, and the self-pulsing behavior. Section VIII discusses the first- and second-order character of the transition from steady-state to the self-pulsing regime. We conclude with Sec. IX, which relates self-pulsing in optical bistability to that in ring lasers and to induced side-mode (probe) gain occuring in extracavity interactions such as in saturation spectroscopy.

## II. MAXWELL-BLOCH EQUATIONS AND THEIR STATIONARY STATES

We consider a ring cavity of total length $\mathcal{L}=2(L+l)$ (Fig. 1). Mirrors 3 and 4 are assumed to have 100% reflectivity. $T$ and $R$ (with $T+R=1$) are the intensity transmittivity and reflectivity of mirrors 1 and 2. An absorber of length $L$ and volume $V'$, and consisting of $N$ two-level atoms, is placed in the cavity. This atomic system is driven by an incident electric field $E_I$ of frequency $\omega_0$. We assume that (i) the atomic system is homogeneously broadened, (ii) the transition frequency of the atoms is equal to $\omega_0$ (i.e., no atomic detuning), and (iii) the length $\mathcal{L}$ of the cavity is equal to an integer number of wavelengths (i.e., no cavity mistuning). That is, we consider purely absorptive optical bistability (OB). The dynamics of the system is ruled by the Maxwell-Bloch equations (MBE)

$$\frac{\partial E}{\partial t}+c\frac{\partial E}{\partial z}=-gP, \tag{2a}$$

$$\frac{\partial P}{\partial t}=\frac{\mu}{\hbar}E\Delta-\gamma_\perp P, \tag{2b}$$

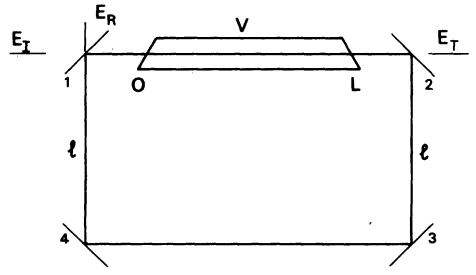


FIG. 1. Unidirectional ring cavity. $E_I$, $E_T$, and $E_R$ are the incident, transmitted, and reflected fields, respectively.

$$\frac{\partial \Delta}{\partial t}=-\frac{\mu}{\hbar}EP-\gamma_\parallel\left(\Delta-\frac{N}{2}\right), \tag{2c}$$

where $P(z,t)$ is the macroscopic polarization field (in terms of the Bloch vector $V$ discussed in the introduction, $P=N\mu V/2\hbar\gamma_\perp$), $\Delta(z,t)$ is one half the difference in population between the lower and upper level, and $E(z,t)$ is the slowly varying envelope of the electric field $\mathcal{E}(z,t)$:

$$\mathcal{E}(z,t)=E(z,t)\exp\left[-i\omega_0\left(t-\frac{z}{c}\right)\right]+\text{c.c.} \tag{3}$$

$\mu$ is the modulus of the dipole moment of the atoms, $g$ is a coupling constant given by

$$g=4\pi\omega_0\mu/V', \tag{4}$$

$V'$ is the volume of the medium, $N$ is the number of active atoms, and $\gamma_\perp$, $\gamma_\parallel$ are the inverses of the population-difference ($T_1$) and dipole ($T_2$) decay times, respectively. The boundary condition appropriate for a ring cavity is[1]

$$E(0,t)=\sqrt{T}E_I+RE(L,t-\Delta t), \tag{5}$$

where $\Delta t=(\mathcal{L}-L)/c$ is the time taken by the light to propagate from mirror 2 to mirror 1. The second term in Eq. (5) describes the feedback contribution, which is an essential ingredient for bistability. The transmitted and reflected fields $E_T$ and $E_R$ are given by

$$E_T(t)=\sqrt{T}E(L,t), \tag{6a}$$

$$E_R(t)=\sqrt{R}\,[E_T(t-\Delta t)-E_I]. \tag{6b}$$

We take $E_I$ real and positive for definiteness. Thus, all the fields in Eqs. (2) can be consistently taken to be real. The stationary solution of Eqs. (2) with boundary condition (5) has been analytically obtained in Ref. 1. It yields the state equation relating the incident and transmitted fields. This relation simplifies drastically in the mean-field limit (1). Introducing for convenience the normalized incident and transmitted field amplitudes $y$ and $x$:

$$y=\frac{\mu E_I}{\hbar(\gamma_\perp\gamma_\parallel T)^{1/2}},\quad x=\frac{\mu E_T}{\hbar(\gamma_\perp\gamma_\parallel T)^{1/2}}, \tag{7}$$

we obtain[7]

$$y=x+\frac{2Cx}{1+x^2}, \tag{8}$$

where $C=\alpha L/2T$, and $\alpha=\mu gN/2\hbar c\gamma_\perp$. As is well known,[7,19] one finds a bistable response for $C>4$ (Fig. 2). The exact analytical solution for OB given in Ref. 1 for the absorptive case has been generalized to the dispersive case (i.e., nonzero atomic and cavity detuning) in Refs. 4, 13, and 20. The most general exact solution, including inhomogeneous broadening (with Lorentzian

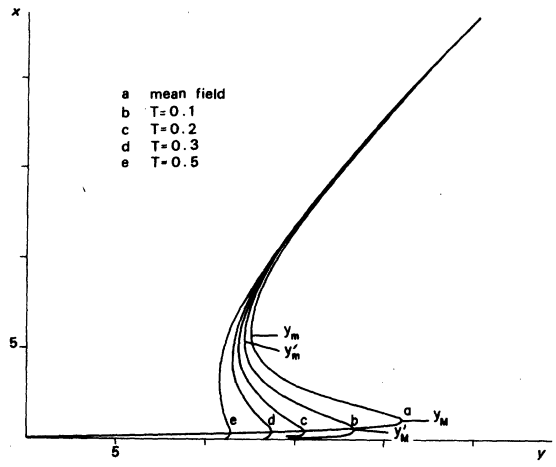


FIG. 2. Transmitted field $x \propto E_T$ as a function of the incident field $y \propto E_I$ for $C=20$ and (a) in the mean-field limit (1), (b) for $\alpha L=4$, $T=0.1$, (c) for $\alpha L=8$, $T=0.2$, (d) for $\alpha L=12$, $T=0.3$, and (e) for $\alpha L=20$, $T=0.5$.

atomic line shape), is given in Ref. 21. A standing-wave formula similar to (8) was given in Ref. 22, which described the monostable problem of a laser with injected signal.

## III. STABILITY ANALYSIS: GENERAL TREATMENT (REF. 2)

A stationary solution is physically meaningful only if it is stable. Thus, it is necessary to perform a stability analysis of the system. Our approach is standard and is based on the linearization of Eqs. (2) around the stationary solution. It is convenient to introduce the dimensionless electric field

$$F(z,t)=\frac{\mu E(z,t)}{\hbar(\gamma_\perp\gamma_\parallel)^{1/2}}\,, \tag{9}$$

so that, with Eqs. (7) and (6a)

$$F(L,t)=x(t)\,. \tag{10}$$

Equations (2) and (5) read then

$$\frac{\partial F}{\partial t}+c\frac{\partial F}{\partial z}=-\frac{\mu g}{\hbar(\gamma_\perp\gamma_\parallel)^{1/2}}P\,, \tag{11a}$$

$$\frac{\partial P}{\partial t}=(\gamma_\perp\gamma_\parallel)^{1/2}F\Delta-\gamma_\perp P\,, \tag{11b}$$

$$\frac{\partial \Delta}{\partial t}=-(\gamma_\perp\gamma_\parallel)^{1/2}FP-\gamma_\parallel\left(\Delta-\frac{N}{2}\right), \tag{11c}$$

and

$$F(0,t)=Ty+RF(L,t-\Delta t)\,. \tag{12}$$

Let us call $F_{st}(z)$, $P_{st}(z)$, and $\Delta_{st}(z)$ a given stationary solution of Eqs. (11). At steady state, Eqs. (11b) and (11c) yield

$$P_{st}(z)=\frac{N}{2}\left(\frac{\gamma_\parallel}{\gamma_\perp}\right)^{1/2}\frac{F_{st}(z)}{1+F_{st}^2(z)} \tag{13}$$

and

$$\Delta_{st}(z)=\frac{N}{2}\,\frac{1}{1+F_{st}^2(z)}\,,$$

while Eq. (11a) gives

$$\frac{dF_{st}}{dz}=-\alpha\frac{F_{st}}{1+F_{st}^2}\,, \tag{14}$$

where

$$\alpha=\mu gN/2\hbar c\gamma_\perp \tag{15}$$

is the linear absorption coefficient. We now introduce small deviations from the stationary values

$$\begin{aligned}\delta F(z,t)&=F(z,t)-F_{st}(z)\,,\\ \delta P(z,t)&=P(z,t)-P_{st}(z)\,,\\ \delta\Delta(z,t)&=\Delta(z,t)-\Delta_{st}(z)\,.\end{aligned} \tag{16}$$

Substituting Eqs. (16) into Eqs. (11) and keeping only the terms linear in the deviations, we obtain the linearized equations

$$\frac{\partial\delta F}{\partial t}+c\frac{\partial\delta F}{\partial z}=-\frac{\mu g}{\hbar(\gamma_\perp\gamma_\parallel)^{1/2}}\delta P\,, \tag{17a}$$

$$\frac{\partial\delta P}{\partial t}=(\gamma_\perp\gamma_\parallel)^{1/2}[F_{st}(z)\delta\Delta+\Delta_{st}(z)\delta F]-\gamma_\perp\delta P\,, \tag{17b}$$

$$\frac{\partial\delta\Delta}{\partial t}=-(\gamma_\perp\gamma_\parallel)^{1/2}[F_{st}(z)\delta P+P_{st}(z)\delta F]-\gamma_\parallel\delta\Delta\,. \tag{17c}$$

Using the boundary condition Eq. (12) and taking into account that $F_{st}(z)$ itself obeys Eq. (12), we obtain the following boundary condition for $\delta F(z,t)$:

$$\delta F(0,t)=R\delta F(L,t-\Delta t)\,. \tag{18}$$

We seek solutions of Eq. (17) of the form

$$\begin{aligned}\delta F_\lambda(z,t)&=\delta F_\lambda(z)\exp(\lambda t)+\text{c.c.}\,,\\ \delta P_\lambda(y,t)&=\delta P_\lambda(z)\exp(\lambda t)+\text{c.c.}\,,\\ \delta\Delta_\lambda(z,t)&=\delta\Delta_\lambda(z)\exp(\lambda t)+\text{c.c.}\end{aligned} \tag{19}$$

We substitute Eqs. (19) into Eqs. (17) and eliminate $\delta P_\lambda(z)$ and $\delta\Delta_\lambda(z)$. With Eq. (13) we then obtain

$$\frac{d\delta F_\lambda}{dz}=-\left(\alpha\Gamma(\lambda,F_{st}(z))+\frac{\lambda}{c}\right)\delta F_\lambda\,, \tag{20}$$

where

$$\Gamma(\lambda, F_{st}(z)) = \frac{\gamma_\perp}{1+F_{st}^2(z)} \frac{\gamma_\parallel[1+F_{st}^2(z)]+\lambda}{(\lambda+\gamma_\perp)(\lambda+\gamma_\parallel)+\gamma_\perp\gamma_\parallel F_{st}^2(z)}. \tag{21}$$

Hence Eqs. (19) and (20) give

$$\delta F_\lambda(z,t) \propto \exp\left[-\alpha\int_0^z dz'\,\Gamma(\lambda, F_{st}(z')) + \lambda\left(t-\frac{z}{c}\right)\right] + \text{c.c.} \tag{22}$$

With the boundary condition (18) we find the equation for $\lambda$:

$$1 = R\exp\left(-\alpha\int_0^L dz\;\Gamma(\lambda, F_{st}(z)) - \frac{\lambda\mathcal{L}}{c}\right), \tag{23}$$

where we have used the definition $\Delta t = (\mathcal{L}-L)/c$. The eigenvalue equation (23) is in turn equivalent to[4]

$$\lambda = -2\pi i n\frac{c}{\mathcal{L}} + \frac{c}{\mathcal{L}}\ln R - \frac{\alpha c}{\mathcal{L}}\int_0^L dz\;\Gamma(\lambda, F_{st}(z)), \tag{24}$$

$$n = 0, \pm 1, \pm 2, \ldots.$$

The structure of Eq. (24) can be simply understood by considering the empty cavity case, i.e., $\alpha = 0$. Equation (24) reduces then to

$$\lambda = -2\pi i n\frac{c}{\mathcal{L}} - \frac{c}{\mathcal{L}}\ln\frac{1}{1-T}. \tag{25}$$

Note that $-(c/\mathcal{L})\ln(1-T)^{-1}$ is the cavity damping constant, which for $T \ll 1$ reduces to the usual expression

$$k = cT/\mathcal{L}. \tag{26}$$

Substituting Eq. (25) into Eq. (22) for $\alpha = 0$, we obtain

$$\delta F_\lambda(z,t) = \text{const}\exp\left[-2\pi i n\left(t-\frac{z}{c}\right)\right] \times \exp\left[-k\left(t-\frac{z}{c}\right)\right] + \text{c.c.} \tag{27}$$

Hence the deviation from the stationary state $\delta F(z,t)$ is a superposition of elementary solutions (27) composed of the cavity running modes $(c/\mathcal{L})2\pi n$ damped by mirror losses. Since $E(z,t)$ is the slowly varying envelope of the electric field [see Eq. (3)], $n=0$ corresponds to the *resonant mode*. In general, the exact eigenvalue equation can be solved numerically by using an iterative procedure (see Sec. VI). However, as is usually the case in optical bistability the problem drastically simplifies in the mean-field limit (1), which we consider in the next section.

## IV. STABILITY ANALYSIS: MEAN-FIELD LIMIT (REFS. 2 AND 3)

In the mean-field limit,[1] the stationary field $F_{st}(z)$ becomes uniform in space and Eq. (10) reduces to

$$F_{st}(z) = x. \tag{28}$$

Hence substituting Eq. (28) into Eq. (24) and using Eqs. (21) and (26) and the definition $C = \alpha L/2T$, we obtain

$$\lambda^3 + c_2\lambda^2 + c_1\lambda + c_0 = 0, \tag{29}$$

where

$$\alpha_n = 2\pi c n/\mathcal{L}, \quad n = 0, \pm 1, \ldots \tag{30}$$

and

$$c_2 = k + \gamma_\perp + \gamma_\parallel + i\alpha_n,$$
$$c_1 = k(\gamma_\perp+\gamma_\parallel) + \gamma_\perp\gamma_\parallel(1+x^2) + \frac{2Ck\gamma_\perp}{1+x^2} + (\gamma_\perp+\gamma_\parallel)i\alpha_n, \tag{31}$$
$$c_0 = k\gamma_\perp\gamma_\parallel\left(1+x^2+2C\frac{1-x^2}{1+x^2}\right) + \gamma_\perp\gamma_\parallel(1+x^2)i\alpha_n.$$

For $n=0$, we recover the cubic equation discussed in Ref. 23 in the framework of the mean-field theory of OB. For $n \neq 0$, Eq. (29) gives the eigenvalues $\lambda$ for the off-resonance modes. We label these eigenvalues with two indices: the index $n$, referring to the $n$th running mode and an index $j = 1,2,3$. For a given $n$, $\lambda_{nj}$ are the three solutions of Eq. (29). Consistently with the mean-field limit, these solutions must be calculated to first order in $T$. One easily obtains (remember that $k \propto T$)

$$\lambda_{n1} = -i\alpha_n - k\left(1+\frac{2C\gamma_\perp}{1+x^2}\frac{\gamma_\parallel(1-x^2)-i\alpha_n}{(\gamma_\perp-i\alpha_n)(\gamma_\parallel-i\alpha_n)+\gamma_\perp\gamma_\parallel x^2}\right) + O(T^2), \tag{32a}$$

$$\lambda_{n2}, \lambda_{n3} = -\tfrac{1}{2}\{\gamma_\perp+\gamma_\parallel \pm [(\gamma_\perp-\gamma_\parallel)^2 - 4\gamma_\perp\gamma_\parallel x^2]^{1/2}\} + O(T). \tag{32b}$$

The stationary solution is stable if and only if $\mathrm{Re}\lambda_{nj} \leq 0$ for all $n$ and $j$. As we see from Eq. (32), for small $T$ one always has $\mathrm{Re}\lambda_{n2}$, $\mathrm{Re}\lambda_{n3} < 0$. Hence the stability is determined by $\lambda_{n1}$. Neglecting terms $O(T^2)$, we have

$$-\frac{\mathrm{Re}\lambda_{n1}}{k} = 1 + \frac{2C\gamma_\perp}{1+x^2}\frac{\gamma_\parallel(1-x^2)[\gamma_\perp\gamma_\parallel(1+x^2)-\alpha_n^2]+\alpha_n^2(\gamma_\perp+\gamma_\parallel)}{[\gamma_\perp\gamma_\parallel(1+x^2)-\alpha_n^2]^2+\alpha_n^2(\gamma_\perp+\gamma_\parallel)^2}. \tag{33}$$

Note, in particular, that for $n=0$

$$\frac{\lambda_{01}}{k}=-\left(1+2C\frac{1-x^2}{(1+x^2)^2}\right)=-\frac{dy}{dx}, \tag{34}$$

where $dy/dx$ is calculated from the state equation (8). Hence, all the stationary states lying on the part of the curve $x=x(y)$ with *negative* slope are unstable because the resonant mode $n=0$ is unstable ($\mathrm{Re}\lambda_{01}>0$). Let us now consider the part of the curve $x=x(y)$ with positive slope. In this region, the resonant mode is always stable, but some off-resonance modes can become unstable. The instability condition $\mathrm{Re}\lambda_{n1}>0$ gives a biquadratic equation for $\alpha_n$. The discussion of this equation leads to the following conclusion. The stationary state is unstable when the following two conditions are simultaneously satisfied:

$$R\geq 0, \quad S+R^{1/2}\geq 0 \tag{35}$$

where

$$R=\gamma_\perp^2\gamma_\parallel^2x^4\left(1-\frac{y}{x}\right)^2+\left(\gamma_\parallel^2-\gamma_\perp^2\frac{y}{x}\right)^2 - 2\gamma_\perp\gamma_\parallel x^2\left(3\gamma_\parallel^2+4\gamma_\perp\gamma_\parallel+\frac{y}{x}(3\gamma_\perp^2-\gamma_\parallel^2)-\gamma_\perp^2\frac{y^2}{x^2}\right) \tag{36}$$

and

$$S=\gamma_\parallel(3\gamma_\perp x^2-\gamma_\parallel)-\frac{y}{x}\gamma_\perp(\gamma_\perp+\gamma_\parallel x^2), \tag{37}$$

provided at least one of the discrete values $\alpha_n$ lies in the interval $\alpha_{\min}<|\alpha_n|<\alpha_{\max}$, where

$$\alpha_{\max,\min}=\frac{1}{\sqrt{2}}(S\pm\sqrt{R}\,)^{1/2}. \tag{38}$$

Note that since $\lambda_{-n}=\lambda_n^*$, the modes become unstable in pairs. We now limit our discussion to the case $\gamma_\perp=\gamma_\parallel\equiv\gamma$, which leads to somewhat simpler algebra. The conditions (35) reduce then to

$$C^2-4x^2\geq 0, \tag{39}$$
$$x^2-(C+1)+(C^2-4x^2)^{1/2}\geq 0.$$

The analysis of Eq. (39) is simple and leads to the following picture, which is illustrated in Fig. 3. For $C>2(1+\sqrt{2}\,)$ the points on the high-transmission branch such that $x<C/2$ are unstable provided that at least one of the discrete values $\alpha_n$ lies in the range $\alpha_{\min}(x)<|\alpha_n|<\alpha_{\max}(x)$, where (cf. Fig. 4)

$$\alpha_{\max,\min}(x)=\gamma[x^2-C-1\pm(C^2-4x^2)^{1/2}]^{1/2}. \tag{40}$$

Note that $\alpha_{\max}(x)$ is always strictly smaller than the Rabi frequency of the transmitted field

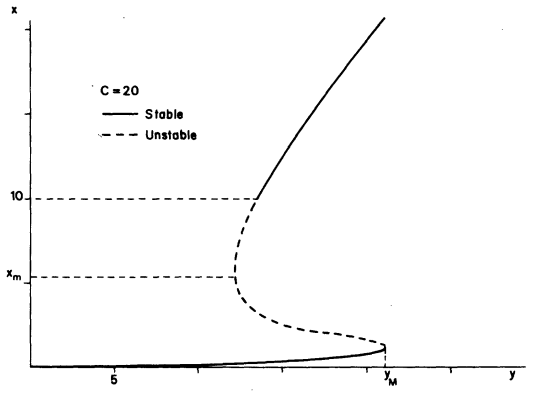


FIG. 3. Stable and unstable steady states in the hysteresis cycle of transmitted vs incident field. Mean-field limit (1), $C=20$, $\gamma_\perp=\gamma_\parallel=\gamma$. The points on the dashed-line part with positive slope are unstable only if at least one of the discrete values $\alpha_n=2\pi nc/\mathcal{L}$ ($n=0,\pm1,\ldots$) lies within the range $\alpha_{\min}(x)<|\alpha_n|<\alpha_{\max}(x)$ (see text and Fig. 4).

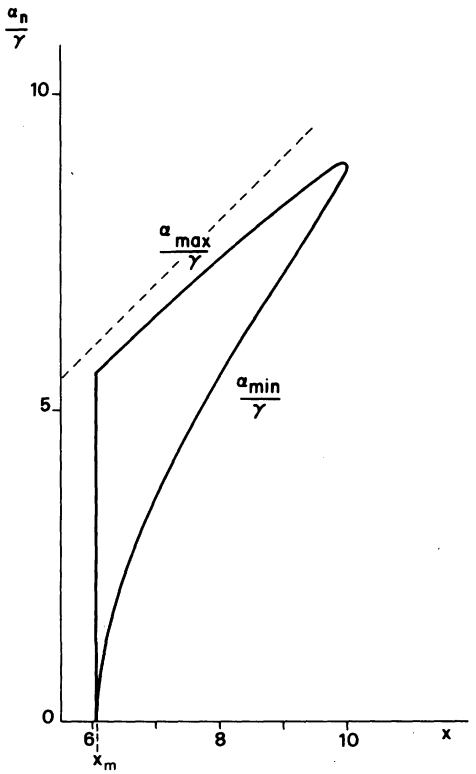


FIG. 4. $\alpha_{\max}$ and $\alpha_{\min}$ as functions of $x$, defining the instability region. We have assumed the mean-field limit, and $\gamma_\perp=\gamma_\parallel=\gamma$ [(Eq. 40)]. The dotted line indicates the Rabi frequency of the transmitted field in units of $\gamma$. For $\gamma_\perp=\gamma_\parallel$, this line is given by $x$ [see Eq. (7)].

$$\Omega_T=\frac{\mu E_T}{\hbar\sqrt{T}}=\gamma x\,,$$

i.e., the frequency of the unstable modes never differs from the frequency of the incident field by an amount larger than the Rabi frequency $\Omega_T$. Note also that since $2(1+\sqrt{2})>4$, one can get instability only when there is a hysteresis cycle. This is no longer true in the case of dispersive OB, where one can obtain an instability also without bistability.[24] This indicates that the dispersive case may be more suitable than the absorptive one for observing self-pulsing.

Returning to the absorptive case, we remark that the picture changes very little for the case $\gamma_{\parallel}=2\gamma_{\perp}$; one finds then that instabilities occur for $x\leq C/2.12$ instead of $x<C/2$. (Note also that for $\lambda_{\parallel}\ll\lambda_{\perp}$, e.g., for heavily pressure broadened systems one never finds instability since no gain is induced.)

The same problem has also been considered in a Fabry-Perot cavity.[25,26] Reference 25 solves the eigenvalue problem for a cavity filled with medium and predicts that the threshold for the onset of an instability is raised very substantially. Reference 26 considers the effects of various possible cavity fill factors and predicts no instability for the filled cavity case. Perhaps the discrepancy is due to the use of a truncated spatial Fourier series in Ref. 25, or to the assumption of Ref. 26 that the real part of the eigenvalues and the side-mode gain are proportional (cf. Sec. IX). Reference 26 also shows that a cavity containing medium only in the ends is subject to instabilities similar to those in the unidirectional ring case, while placement of medium only in the middle has no gain instability. These results are easily understood in terms of multimode spatial-hole burning.[26]

## V. COMPARISON OF THE EXACT AND THE MEAN-FIELD EIGENVALUE EQUATION

In the following, we measure the time in units of $L/c$. Accordingly we use the quantities

$$\lambda'_{nj}=\lambda_{nj}L/c,\quad \alpha'_n=\alpha_n\frac{L}{c}=\frac{2\pi nL}{\mathfrak{L}},\quad \gamma'=\gamma\frac{L}{c}\,, \tag{41}$$

etc. From (33) we have for $\gamma_{\perp}=\gamma_{\parallel}=\gamma$:

$$\mathrm{Re}\lambda'_{n1}=-\frac{TL}{\mathfrak{L}}\left(1+\frac{2C}{1+x^2}\left\{(1-x^2)\left[1+x^2-\left(\frac{\alpha'_n}{\gamma'}\right)^2\right]+2\left(\frac{\alpha'_n}{\gamma'}\right)^2\right\}\Bigg/\left\{\left[1+x^2-\left(\frac{\alpha'_n}{\gamma'}\right)^2\right]^2+4\left(\frac{\alpha'_n}{\gamma'}\right)^2\right\}\right). \tag{42}$$

Furthermore, Eq. (40) reads

$$\alpha'_{\max,\min}=\gamma'[x^2-C-1\pm(C^2-4x^2)^{1/2}]^{1/2}. \tag{43}$$

From (42) and (43) we note the following properties:

(1) $\mathrm{Re}\lambda'_{n1}$ depends on $\alpha'_n$ and $\gamma'$ only in the ratio $\alpha'_n/\gamma'$.

(2) $\alpha'_{\max}$ and $\alpha'_{\min}$ are independent of $\mathfrak{L}$, $L$, and $T$ (for $C$ fixed).

(3) $\alpha'_{\max}$ and $\alpha'_{\min}$ are proportional to $\gamma'$ (for $C$ fixed).

(4) If one plots $\mathrm{Re}\lambda'_{n1}$ vs $\gamma'$ for $\alpha'_n$ fixed, the values of $\gamma'$ such that $\mathrm{Re}\lambda'_{n1}=0$ are proportional to $n$. In fact, the condition $\alpha'_{\min}<\alpha'_n<\alpha'_{\max}$ is equivalent to

$$2\pi\frac{L}{\mathfrak{L}}\left(\frac{\gamma'}{\alpha'_{\max}}\right)n<\gamma'<2\pi\frac{L}{\mathfrak{L}}\left(\frac{\gamma'}{\alpha'_{\min}}\right)n\,, \tag{44}$$

where according to property (3) $\gamma'/\alpha'_{\max,\min}$ is independent of $\gamma'$.

Let us now consider the exact eigenvalues. They are solutions of the exact eigenvalue equation (24), which for $\gamma_{\perp}=\gamma_{\parallel}=\gamma$ reduces to

$$\lambda'_{n1}=-i\alpha'_n+\frac{L}{\mathfrak{L}}\left(\ln(1-T)-2CT\int_0^1 d\xi\,\frac{1-F_{\mathrm{st}}^2(\xi L)+\lambda'_{n1}/\gamma'}{[1+F_{\mathrm{st}}^2(\xi L)][(\lambda'_{n1}/\gamma'+s)^2+F_{\mathrm{st}}^2(\xi L)]}\right), \tag{45}$$

where

$$\xi=z/L\,. \tag{46}$$

The property (1) is clearly no longer true. In order to find $\alpha'_{\max}$ and $\alpha'_{\min}$, let us consider $\alpha'_n$ as a continuous variable and set $\mathrm{Re}\lambda'_{n1}=0$, i.e., $\lambda'_{n1}=i\nu$, with $\nu$ real. By substituting this position into Eq. (45) and equating real and imaginary parts, we obtain

$$0=\ln(1-T)-2CT\int_0^1 d\xi\,\mathrm{Re}\left(\frac{1-F_{\mathrm{st}}^2(\xi L)+i\nu/\gamma'}{[1+F_{\mathrm{st}}^2(\xi L)][(i\nu/\gamma'+1)^2+F_{\mathrm{st}}^2(\xi L)]}\right), \tag{47a}$$

$$\frac{\alpha_n'}{\gamma'} = -\frac{\nu}{\gamma'} - 2CT\frac{L}{\mathcal{L}\gamma'}\int_0^1 d\xi\,\mathrm{Im}\left(\frac{1-F_{st}^2(\xi L)+i\nu/\gamma'}{[1+F_{st}^2(\xi L)][(i\nu/\gamma'+1)^2+F_{st}^2(\xi L)]}\right). \tag{47b}$$

Equation (47a) is a closed equation for $\nu$. The solutions of (47a) are substituted into (47b), which gives $\alpha_n'$, i.e., $\alpha_{max}'$ and $\alpha_{min}'$. The solutions of (47b) depend on $T$ [because in general $\ln(1-T)\neq -T$] and on $L$ [via $F_{st}(\xi L)$]. On the other hand, the solutions of (47a) are independent of $\mathcal{L}$ and proportional to $\gamma'$. However, these last two properties do not hold for $\alpha_{max,\,min}'$, as one sees from (47b). One only recovers (2) and (3) in the mean-field limit (1), for which (i) $\ln(1-T)\simeq -T$, (ii) $F_{st}=x$ does not depend on $z$, and (iii) $\alpha_n'\simeq -\nu$. Furthermore, since $\alpha_{max,\,min}'$ are no longer proportional to $\gamma'$, the property (4) is in general no longer valid. Of course, the degree of violation of these properties depends on how far we are from the mean-field limit. Note in particular that the independence of $\alpha_{max,\,min}$ from $\mathcal{L}$ (property 2) has practical importance. In fact, the easiest way of varying the mode frequencies $\alpha_n$ is to vary the total length $\mathcal{L}$ of the cavity. In the mean-field limit, in which $\alpha_{min}$ and $\alpha_{max}$ are independent of $\mathcal{L}$, we can bring an arbitrary number of modes inside the instability region simply by varying $\mathcal{L}$. The same does not necessarily hold in general since the boundaries are themselves functions of $\mathcal{L}$.

## VI. NUMERICAL CALCULATIONS OF THE EXACT EIGENVALUES

In this section we calculate numerical solutions of the eigenvalues (45) outside the range of validity of the mean-field limit (1). To give a rough idea, for $C=20$, the results obtained in the mean-field limit of Eq. (32a) are practically exact for $T=0.01$. We work away from this limit by considering mirror transmissions $T=0.1$, 0.2, 0.3, and 0.5, while retaining $C=20$ and $\mathcal{L}/L=5$. We solve the transcendental eigenvalue equation (45) using an iterative procedure. Specifically, we begin by inserting the appropriate mean-field eigenvalue into the integrand of (45) and calculating an improved eigenvalue. This improved value is used, in turn, in the integrand to obtain a still better value, etc. Once $T$ and $C$ are chosen, $\alpha L=2CT$ is also chosen. For a given $y$, or more precisely for a given $x$ in the high-transmission branch, the internal field $F_{st}(\xi L)$ is also fixed, because it depends on $L$ only in the combination $\alpha L$. Hence the only remaining variables in (45) are $\gamma'$ and $\alpha_n'$. We have graphed Eq. (45) for several values of these parameters, as shown in Figs. 5–14. Figure 5 shows the variation of the exact eigenvalue $\lambda_{01}'$ (corresponding to the resonant mode $\alpha_n'=0$) when $x$ runs along the high-transmission branch (for $T=0.1$, $\gamma'=0.2$). In the same figure, the exact eigenvalue $\lambda_{01}'$ is compared to its mean-field-limit counterpart given by Eq. (34). The figure shows that $\lambda_{01}$ vanishes at the lower-bistability threshold, which for $T=0.1$ is $x_m=5.58$. This implies that $\lambda_{01}$ becomes positive for that part of the curve $x=x(y)$ having negative slope, as one expects. Figure 6 illustrates the variation of the real part of the eigenvalue $\lambda_{11}'$ (corresponding to the first adjacent mode $\alpha_1$) as a function of $\gamma'$ for fixed $x$ and $T=0.1$.

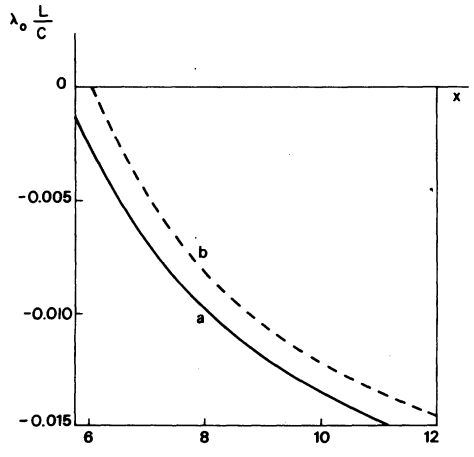


FIG. 5. Resonant mode eigenvalue $\lambda_{01}$ (labeled $\lambda_0$ here) as a function of $x$: (a) Exact as obtained numerically from Eq. (45) for $T=0.1$, and $\gamma L/c=0.2$, (b) and mean-field result for $T\ll 1$ [see Eq. (36)]. In this figure and Figs. 6–14, we take $C=20$, $\mathcal{L}/L=5$, and $\gamma_\perp=\gamma_\parallel=\gamma$.

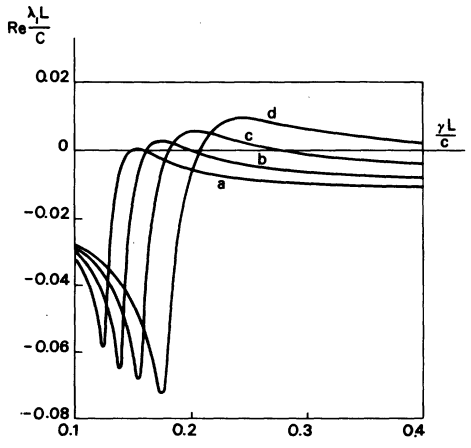


FIG. 6. Real part of the adjacent mode eigenvalue [exact as derived from Eq. (45)] $\lambda_{11}$ as a function of $\gamma L/c$ for $T=0.1$. (a) $x=9$, (b) 8, (c) 7, and (d) 6.

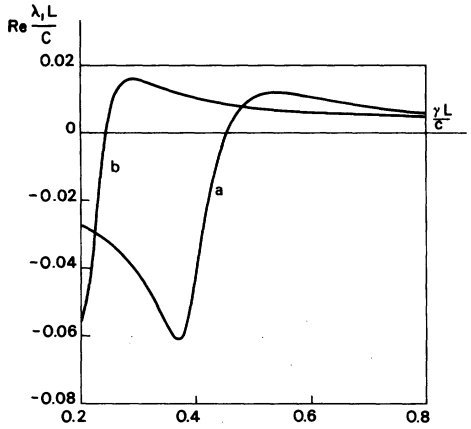


FIG. 7. Real part of the adjacent mode eigenvalue $\lambda_{11}$ as a function of $\gamma L/c$ for $x=6$. (a) Exact for $T=0.1$ obtained from Eq. (45) and (b) mean-field result for $T \ll 1$ [Eq. (42)].

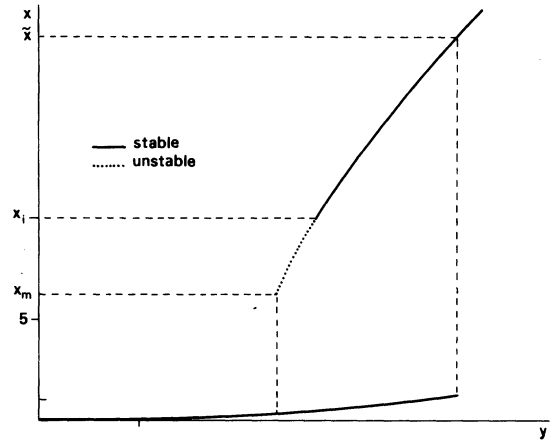


FIG. 9. Stable and unstable steady states in the hysteresis cycle of transmitted vs incident light for $T=0.1$. $x_i$, $x_m$, and $\tilde{x}$ are used to define $\mathcal{R}$.

Note the sharp minima of these curves, which are absent in the corresponding mean-field-limit curves obtained from Eq. (42) as shown in Fig. 7.

From curves of the type shown in Fig. 7, one obtains the instability regions of the mode $\alpha_1$ for $T=0.1$ to be compared with those for the mean-field limit shown in Fig. 4. The exact instability region is obtained by finding the range of $\alpha_1'/\gamma'$ characterized by $\mathrm{Re}\lambda_{11}'>0$ for each value of $x$. Figure 8 plots the results. Figure 9 reproduces the steady-state curve $x(y)$ for $T=0.1$ as given in Fig. 2, here with the unstable part of the high-transmission branch indicated by a dotted line. The exact instability region of $\alpha_1/\gamma'$ for $T=0.1$ is also obtained in Sec. VII by numerically solving the Maxwell-Bloch equations. The agreement between that calculation and Fig. 8 is excellent.

Figures 10, 11, and 12 are analogous to Fig. 6, but for $T=0.2$, 0.3, and 0.5. In this connection it is interesting to consider the variation of the instability-bistability ratio $\mathcal{R}=(x_i-x_m)/(\tilde{x}-x_m)$ as

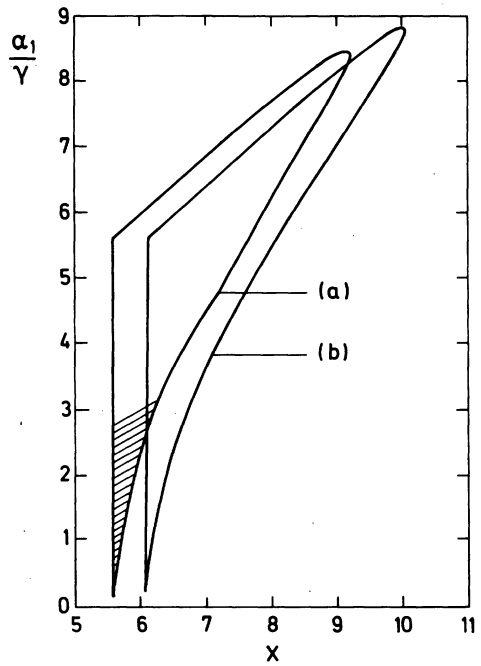


FIG. 8. Numerically determined instability region for $T=0.1$, $C=20$, $\mathcal{L}/L=5$, and $\gamma_\perp=\gamma_\parallel=\gamma$. The shaded part indicates the region where both $\alpha_1$ and $\alpha_2$ (and sometimes other modes) are unstable. The curve (b) shows for comparison the instability region in the mean-field limit as given in Fig. 4.

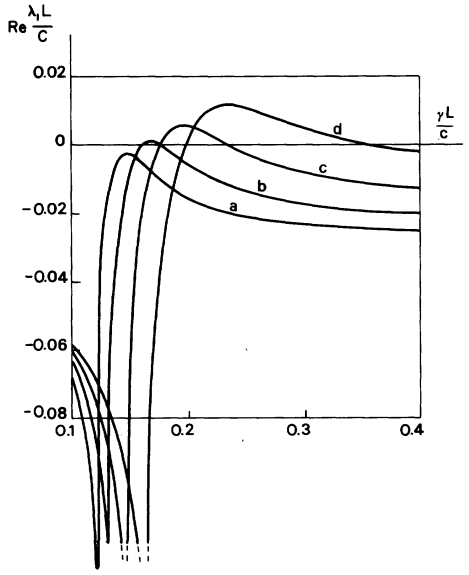


FIG. 10. Same as Fig. 6, but with $T=0.2$.

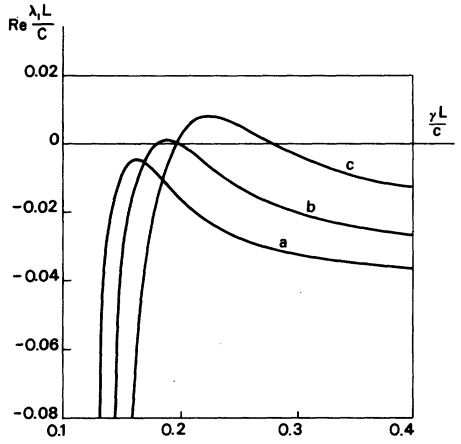


FIG. 11. Same as Fig. 6, but with $T=0.3$, (a) $x=8$, (b) 7, and (c) 6.

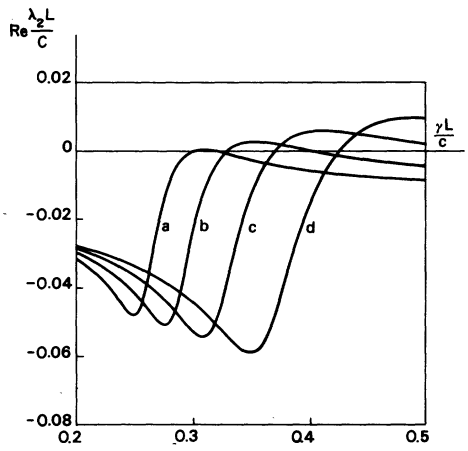


FIG. 13. Real part of the eigenvalue $\lambda_{21}$ corresponding to the mode $\alpha_2$ [exact as obtained from Eq. (45)] as a function of $\gamma L/c$ for $T=0.1$, (a) $x=9$, (b) 8, (c) 7, and (d) 6.

a function of $T$. One finds $\mathfrak{R}=0.3$ for $T \ll 1$ (mean-field limit), $\mathfrak{R}=0.35$, 0.42, and 0.52 for $T=0.1$, 0.2, and 0.3, respectively. Hence increasing $T$ reduces the range of instability, but it reduces the range of optical bistability even faster. This suggests the possibility that instabilities may exist in the absence of bistability. It is difficult to check this possibility because of numerical anomalies for $T > 0.5$.

Figure 13 is similar to Fig. 6, but plots $\mathrm{Re}\lambda'_{21}$ rather than $\mathrm{Re}\lambda'_{11}$ vs $\gamma'$ for fixed $x$ and $T=0.1$. Note that the values of $\gamma'$ occurring for $\mathrm{Re}\lambda'_{21}=0$ and $\mathrm{Re}\lambda'_{11}=0$ are not strictly proportional to the mode index $n$, as one expects in the mean-field limit of Eq. (44). This point is discussed analytically in Sec. IV. Figure 14 (with $\gamma=1$) carries this point further by graphing $\mathrm{Re}\lambda'_{n1}$ vs $\alpha'_n$ for fixed $x$, $T=0.1$. Comparison with the same curves except for $\gamma'=0.2$ reveals differences in the peaks, valleys, and zero-crossing points of up to several percent. Note that in Fig. 14, $\mathrm{Re}\lambda_{n1}=0$ for $x=5.58$ and $\alpha_n=0$ (resonant mode) in agreement with Fig. 5.

By iteratively solving the exact eigenvalue equation (24), we see that the real part of the eigenvalue $\lambda'_{n1}$ has the structure

$$\mathrm{Re}\lambda'_{n1}=G(F_{st},\alpha_n)-\frac{c}{\mathcal{L}}\ln\frac{1}{1-T}\ , \tag{48}$$

where $G$ has been calculated numerically as described in Sec. V. The mean-field value of $G$ follows immediately from Eq. (33). The second term on the rhs of Eq. (48) represents the cavity

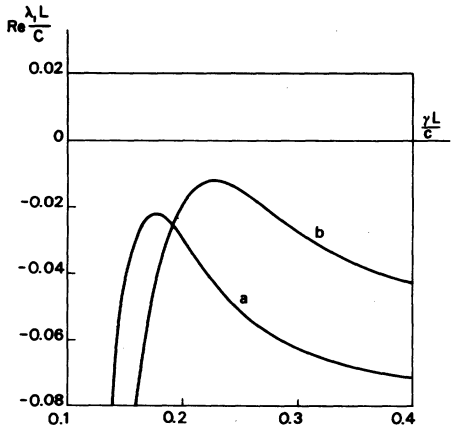


FIG. 12. Same as Fig. 6, but for $T=0.5$, (a) $x=8$ and (b) $x=7$.

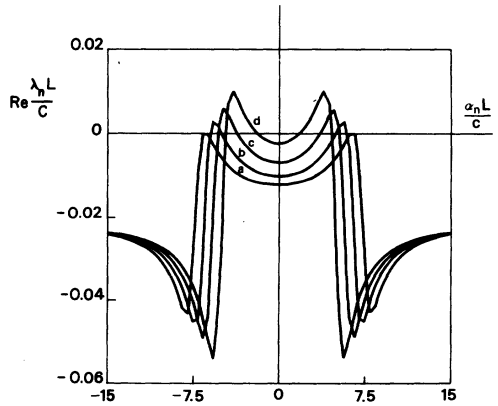


FIG. 14. Real part of the eigenvalue $\lambda_{n1}$ as a function of $\alpha_n$ (treated as a continuous variable) as obtained from the exact equation (45) for $T=0.1$, $\gamma L/c=1$. (a) $x=9$, (b) $x=8$, (c) $x=7$, and (d) $x=6$.

losses. The $G$ term results from the induced polarization of the medium and gives gain when positive, loss when negative. For $\mathrm{Re}\lambda'_{n1} > 0$, the gain exceeds the loss, so that the $n$th mode is amplified and the single-mode operation is unstable. In this situation, our system behaves as a novel type of laser that works without population inversion. Part of the resonant mode's (mode 0) energy is transferred through the nonlinear response to the side modes, giving them gain. As in the usual laser problem, spontaneous emission provides the initial impetus to side-mode buildup. This is the origin of the multimode, self-pulsing behavior of our system. The buildup is complicated by the fact that the system may be near a phase transition. We now consider the time development of this buildup by integrating the coupled Maxwell-Bloch equations in time.

## VII. NUMERICAL ANALYSIS OF THE TIME-DEPENDENT MAXWELL-BLOCH EQUATIONS

The observation that certain eigenvalues may become positive is in itself insufficient to determine the general time development of the system. For this we integrate the exact coupled Maxwell-Bloch equations (11) numerically.

As shown in Ref. 3, the existence of unstable steady states in the high-transmission branch (see Fig. 3) can lead to two different types of behavior, depending upon the precise values of the parameters. In the first case the system precipitates to the (stable) stationary state on the low-transmission branch corresponding to the incident field $y$ [see Fig. 15, part (2)]. The second and more interesting possibility is that the system evolves to a time periodic state (limit cycle). The transmitted light consists then of an undamped regular sequence of pulses [self-pulsing, see Fig. 15, part (1)]. There is *a priori* a third possibility, namely, the system evolves to a

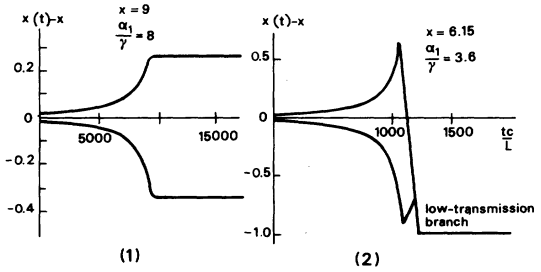


FIG. 15. Envelope of the difference $x(t) - x$ between the transmitted field and its stationary value for two cases in which the stationary state in the high-transmission branch is unstable. $T = 0.1$, $C = 20$, $\mathcal{L} = 5L$, and $\gamma_\perp = \gamma_\parallel = \gamma$. The time is in units of $L/c$.

chaotic situation in which it exhibits a completely irregular sequence of pulses. Until now, we have not found any evidence for this type of behavior. Examples of chaotic behavior in OB have recently been reported.[13-15] However, they occur in dispersive cases and quite far from the mean-field limit. Note that in Fig. 15, we have drawn only the *envelope* of the transmitted light $x(t)$, which actually oscillates with a frequency roughly equal to the difference $2\pi c/\mathcal{L}$ between the adjacent unstable-mode frequency and the resonant-mode frequency. The numerical analysis of the instability has been performed via a direct solution of the Maxwell-Bloch equations (11), using a Runge-Kutta algorithm.[10]

We limit our discussion mostly to the set of parameters $C = 20$, $T = 0.1$, $\alpha L = 4$, and $\mathcal{L}/L = 5$. Although this value of the mirror transmission is too high to fulfill the mean-field conditions (1), this choice is guided by the need to keep the computer time within reasonable limits. Note that as the mean-field limit (1) is approached, the time taken by the bistable system to reach a limit cycle increases significantly. For this limit we could use the multimode ring laser theory of Ref. 27, appropriately modified for the injected signal boundary conditions and change in sign of the linear gain coefficient or the new propagation equations, equivalent for the Maxwell-Bloch equations in the mean-field limit (1), derived by one of us (Ref. 28, Sec. 3).

### A. Instability region

Section VI has determined the region of instability (Fig. 8) by iterating the exact eigenvalue equation (45). Here we have used an alternative approach based on direct integrations of the Maxwell-Bloch equations. We have determined the range of parameters (driving field and cavity length) for which the mode adjacent to the resonant mode becomes unstable. (In the following, we label this mode by its difference in frequency $\alpha_1 = 2\pi c/\mathcal{L}$ with respect to the resonant mode.) Our numerical analysis proceeds along the following lines: We first calculate the stationary solution $F_{st}(z)$ in the high-transmission branch for a given value of the driving field $y$. We then choose the initial conditions for the Maxwell-Bloch equations such that (a) the deviation $\delta F$ from the stationary value $F_{st}(z)$ is initially small (b) the vector

$$\begin{pmatrix} \delta F \\ \delta P \\ \delta \Delta \end{pmatrix}$$

is initially the eigenstate of the linearized prob-

lem (17) corresponding to the eigenvalue $\lambda_{11}$ (or more precisely the approximate expression of this eigenstate obtained in the mean-field limit). This guarantees that only the adjacent mode $\alpha_1$ is initially excited. The first stage of the time evolution is then ruled by the linearized equations (17). Hence in the initial stage the deviation of the transmitted field from its stationary value $x(t)-x$ is either exponentially damped or grows exponentially depending upon whether $\alpha_1$ is stable or unstable. The whole instability region is then obtained by scanning the driving field $y$ and the parameter $\alpha_1/\gamma=2\pi c/5L\gamma$. The instability region obtained by this numerical technique coincides exactly with that obtained by the eigenvalue analysis of Sec. VI. The shaded part of Fig. 8 is the region where not only the adjacent mode $\alpha_1$, but also the next mode $\alpha_2$ is unstable. This is quite obvious, since when $\alpha_1/\gamma$ lies in that shaded region, then $\alpha_2/\gamma=2\alpha_1/\gamma$ also falls within the instability region. Similarly, when $\alpha_1$ lies even further down in the instability region, the next modes $\alpha_3$, $\alpha_4$, etc., become successively unstable.

### B. Precipitation region

Once the instability region is determined, the question remains as to what kind of dynamics is associated with the existence of unstable modes. As already mentioned, we have found that, depending upon the driving field $y$ and $\alpha_1/\gamma$, the system either reaches a limit cycle or precipitates down to the low-transmission branch. In Fig. 16, we show the domains of the instability region leading to one or the other of these possibilities. They were determined by directly solving the Maxwell-Bloch equations (11). We first note that the lower part of the instability region, i.e., the region where the mode $\alpha_2$ is also unstable, is entirely contained within the precipitation domain. We have numerically investigated several points in this region. To make sure that the type of dynamics is independent of the initial conditions, we have considered three possibilities: (1) only the mode $\alpha_1$ is initially excited, (2) only the mode $\alpha_2$ is initially excited, and (3) both modes are initially excited. In all cases we have obtained precipitation (the precipitation time depends, however, on the initial condition).

### C. Self-pulsing region

In the remainder of this section, we limit our discussion to the limit cycle (self-pulsing) region, which is the most interesting one, at least from the point of view of device applications. Supposing that one moves into the self-pulsing domain from somewhere within the precipitation region, one may first ask what happens when one crosses the boundary between them. We have found that this transition is characterized by the fact that near the boundary, the approach to the limit cycle is extremely slow, and the envelope of $x(t)$ exhibits a large number of slow oscillations (Fig. 17). As one goes further into the self-pulsing region (say, along a horizontal line in Fig. 16), these pulsations become less pronounced, and the approach to a limit cycle becomes increasingly faster. Eventually, the pulsations disappear altogether.

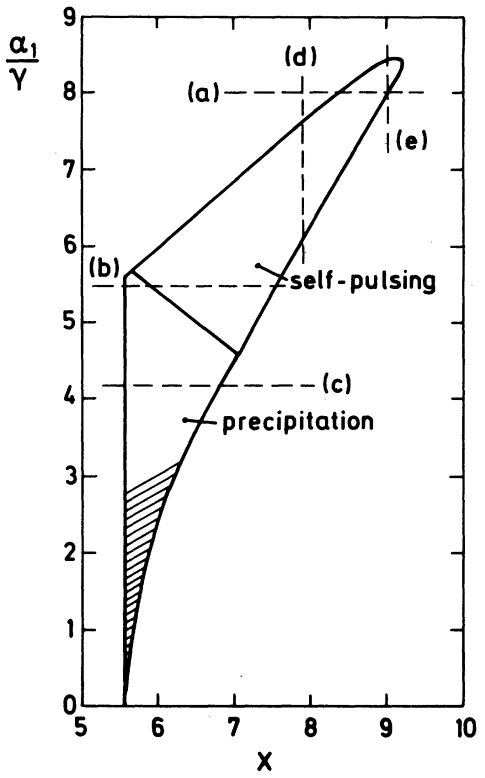


FIG. 16. Subdivision of the instability region (Fig. 8) into self-pulsing and precipitation regimes. The lines (a)–(e) are discussed in connection with Figs. 19 and 20.

Let us now describe the main features of the self-pulsing behavior. As already mentioned, the frequency of the oscillations is roughly equal to $\alpha_1$, with a deviation from this value proportional to $T$, i.e., of the order of 10%. The mean value $\bar{x}$ of the oscillations is always lower than the unstable steady-state value. This may be interpreted as due to a kind of attraction exerted by the stable steady state. Intuitively, one may argue that it is applied by the resonant mode, which is the only excited one when the system is at steady state. One expects the attraction to be larger, the smaller the difference $\alpha_1$ between the

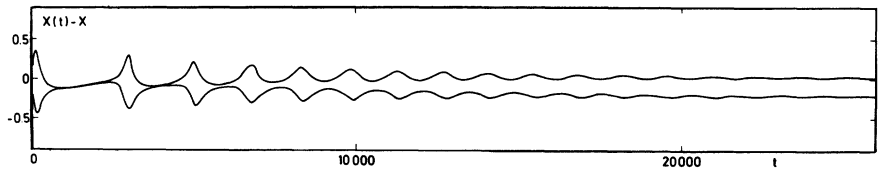


FIG. 17. Envelope of the difference $x(t)-x$ between the transmitted field and its stationary value for $x=6$, $\alpha_1/\gamma=5.5$, $T=0.1$, $C=20$, $\mathfrak{L}=5L$, and $\gamma_\perp=\gamma_\parallel=\gamma$. Time is given in units of $L/c$.

frequency of the unstable mode and that of the resonant mode. This is consistent with the fact that $x-\bar{x}$ increases when $\alpha_1$ decreases. When $\alpha_1$ becomes small enough, the attraction of the low-transmission steady state becomes overwhelming and the system precipitates. This intuitively explains the position of the precipitation region.

Figure 18 shows the profile of the field $F(z,t)$ inside the sample for eight different times within one period of oscillations, when the limit cycle has been reached. To a first approximation, the curves in Fig. 18 may be fitted by the expression

$$F(z,t)=\bar{x}+A\cos[\Delta\omega(t-z/v)+\phi_0], \qquad (49)$$

where $A$ and $\Delta\omega\simeq\alpha_1$ are the half-amplitude and the frequency of the oscillations, respectively, and $\phi_0$ is a phase which depends on the initial conditions. The propagation velocity $v$ turns out to be somewhat smaller than the light velocity. From Eq. (3) we see then that the (nonslowly varying) electric field behaves roughly as

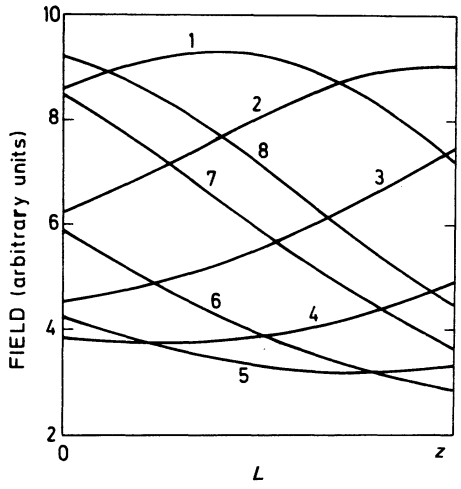


FIG. 18. Field propagation inside the absorber in the self-pulsing regime. We have taken $\gamma_\perp=\gamma_\parallel=\gamma$, $T=0.1$, $C=20$, $\mathfrak{L}=5L$, $x=7.4$, and $\alpha_1/\gamma=5.5$. (1) $t=1400$, (2) $t=1400.7$, (3) $t=1401.4$, (4) $t=1402.1$, (5) $t=1402.8$, (6) $t=1403.5$, (7) $t=1404.2$, and (8) $t=1404.9$ (in units of $L/c$).

$$\mathcal{E}(z,t)\simeq\bar{\mathcal{E}}\cos[\omega_0(t-z/c)] + a\{\cos[(\omega_0+\alpha_1)(t-z/c)+\phi_0] + \cos[(\omega_0-\alpha_1)(t-z/c)-\phi_0]\}, \qquad (50)$$

where we have introduced some obvious symbols and have taken into account that $v\simeq c$ and $\Delta\omega\simeq\alpha_1$. Hence, when the adjacent modes $n=\pm1$ are unstable, part of the incident light is transferred from the resonant mode, of frequency $\omega_0$, to the adjacent modes, of frequencies $\omega_0\pm\alpha_1$. This gives rise to the undamped pulsing behavior (50).

Equations (50) shows that in the self-pulsing regime the dominant contributions to the field come from the resonant mode and the adjacent modes. More generally, when the system is in the instability region, the dynamics involves a competition between the resonant mode and the unstable modes: When the unstable modes prevail, the system approaches the undamped spiking regime; when the resonant mode dominates the dynamics, the system precipitates to the low-transmission branch.

## VIII. ORDER OF THE PHASE TRANSITIONS

We now address the question of the character of the transition from the steady-state regime to the self-pulsing regime, when we cross the boundary of the instability region. For definiteness, let us consider first the following situation. We start from some value of the incident field $y$ larger than $y'_M$ (Fig. 2) such that the system is at steady state in the high-transmission branch. We then slowly decrease the incident field and penetrate into the instability region. If all other parameters are kept fixed, this corresponds to moving from right to left along horizontal lines in Fig. 16. Figure 19(a) illustrates what happens when we move along the line (a). When the point $(x,\alpha_1/\gamma)$ penetrates from the right into the instability region, the self-pulsing behavior appears *abruptly*: The oscillations immediately have a finite amplitude, and the difference $x-\bar{x}$ is finite. Hence, when crossing the right boundary of the instability region the system exhibits a *first*-order-like phase transition from a stationary to a self-pulsing be-

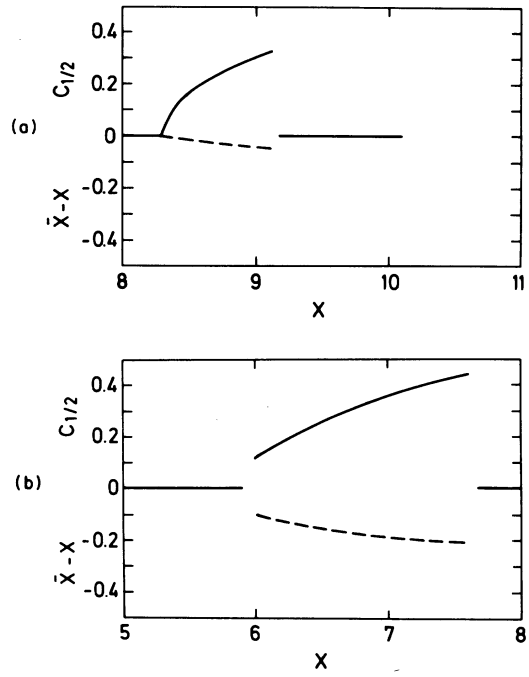


FIG. 19. Variation of the half-amplitude of the pulses (full line) and of $\bar{x}-x$ (mean value of the oscillations minus stationary value, broken line) along the horizontal lines (a) $(\alpha_1/\gamma=8)$ and (b) $(\alpha_1/\gamma=5.5)$ of Fig. 8.

havior. When $y$ (i.e., $x$) is decreased, the amplitude of the oscillations (as well as the difference $x-\bar{x}$) decreases until the oscillations vanish continuously at the left boundary of the instability region. The system is back again in a stable stationary state on the high-transmission branch. Hence crossing the left boundary one finds a *second*-orderlike phase transition from self-pulsing to stationary behavior. If $y$ further decreased below the lower-bistability threshold $y=y'_m$ (Fig. 2), the system jumps to the low-transmission branch as usual.

Let us now follow the system along (b) in Fig. 16. The results are summarized in Fig. 19(b). When we cross the left boundary everything happens as in the previous case (first-order phase transition). However, before arriving at the left boundary, the system reaches the precipitation region and jumps "prematurely" to the low-transmission branch. Finally, in the case $c$, the system precipitates as soon as it enters the instability region. In this case one has no appearance of self-pulsing and the presence of the instability only leads to a net reduction of the hysteresis cycle.

For completeness, we now present results obtained when moving along a vertical line in Fig. 16. This would correspond in practice to keeping $y$ constant and varying $\alpha_1$. This can be achieved by changing the total length $\mathcal{L}$ of the ring cavity. Figures 20(a) and 20(b) show the results of this procedure for two different values of $y$, corresponding to the vertical lines (d) and (e) in Fig. 16. Again, one finds a first-order phase transition when crossing the lower (i.e., right) boundary of the instability region and a second-order transition when crossing the upper (i.e., left) boundary.

Since in a numerical analysis one only considers a discrete set of points, the question arises as to with what certainty one can assert the order of the transition. We have analyzed a considerable number of points in the vicinity of the transition, so that our confidence in the numerical results is very high. Furthermore, we have recently given an analytical treatment of self-pulsing which confirms the validity of our conclusions. It is based on Haken's theory of phase transitions in systems far from thermal equilibrium[29] which we have generalized and applied to OB.[16] In this approach one derives from the Maxwell-Bloch equations an approximate, closed equation for the time evolution of the amplitude $R(t)$ of the unstable mode, which acts as the order parameter in this problem. This equation has the form

$$\dot{R}=-\frac{dV}{dR}\,, \tag{51}$$

where

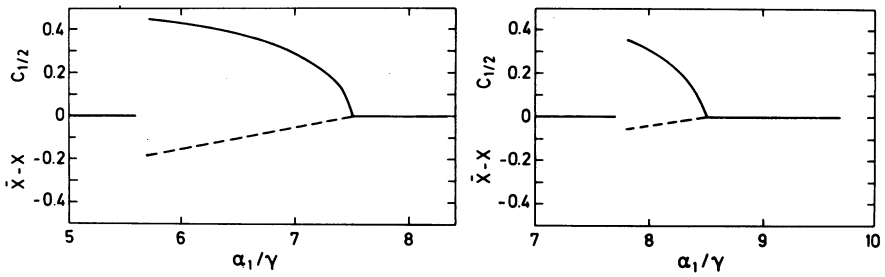


FIG. 20. Same as Fig. 19, but along the vertical lines in Figs. 8(d) $(x=7.7)$ and 8(e) $(x=9)$.

$$V(R) = -(\mathrm{Re}\lambda_{11})R^2/2 + aR^4 + bR^6 .$$

$a$ and $b$ are complicated functions of the driving field $x$ and of the system parameters. $V$ plays the role of a generalized free energy. The nontrivial minimum of $V$ gives directly the half-amplitude $A$ of the oscillations [see Eq. (49)]. This method works only in the mean-field limit (1). For $C=20$ and $T=0.01$, the agreement between analytical and numerical data is satisfactory only when the amplitude of the oscillations is sensibly smaller than the stationary intensity.[17] A substantial improvement is obtained in Ref. 18, where the adiabatic elimination is performed exactly, thereby obtaining a description that works in the whole instability region. One finds a first-order transition at the lower (right) boundary of the instability region (which for $T=0.01$ practically coincides with the mean-field instability region given in Fig. 4) and a second-order transition at the upper (left) boundary. Since there is no reason to believe that a drastic change should occur between $T=1$ and 10%, we consider this result as an independent check of the numerical results presented here.

## IX. DISCUSSION

We have shown that self-pulsing in absorptive optical bistability is due to the onset of instabilities in the side modes of the cavity. These instabilities arise because the nonlinear medium transfers energy from the large centrally tuned mode to the side modes which then grow at the expense of the large mode. If the central mode nevertheless dominates, the system precipitates down to the lower-transmission branch, leading to a net reduction of the size of the hysteresis cycle. Alternatively, the side modes grow and the system reaches a limit cycle characterized by a periodic transmitted field. For this case, the bistable system acts as a cw to pulsed-light converter.

The gain phenomenon has been discussed theoretically[30-35] and experimentally[36,37] for two or more modes interacting outside a cavity. There the side modes called probes are introduced explicitly, rather than building up from spontaneous emission. In the saturation spectroscopy interpretation[34,35] the probe wave derives gain from the saturator wave (mode 0 in our present context) via a parametric interaction resulting from induced population pulsations. Alternatively, the Hamiltonian including the saturator wave can be diagonalized, yielding levels split by the dynamic Stark effect. With either interpretation, field modes passing through such a saturated absorber experience gain for appropriate combinations of detuning, decay constants, etc.

Apart from a proportionality constant, the mean-field-limit value of (48) (Ref. 35) reduces to the $AM$ three-mode formula (13) of Ref. 34 in the case of resonant saturator tuning. Specifically two probes occur since in the cavity two symmetrically placed side modes are involved. The gain that either one experiences is enhanced by the presence of the other, even though neither side mode is assumed to saturate the medium. This surprising result occurs because the side modes act together with the saturator in generating population pulsations, which, in turn, scatter saturator energy into both the side modes. Reference 33 has discussed a gain formula that reduces to the mean-field value of Eq. (48) in some detail, and generalizes the calculation to various degrees of inhomogeneous broadening. The gain phenomenon decreases in magnitude as the inhomogeneous broadening is increased.

In the present problem, the modes interact in a cavity. This differs in important ways from interaction outside a cavity. The side modes build up in a self-consistent way from spontaneous emission, subject to mode pulling and cavity loss considerations familiar in laser theory.[38] As such their direction, frequency, and amplitude are chosen by the cavity boundary conditions, the absorber and the input wave, rather than directly by the experimenter. This fact is particularly relevant as one departs from the mean-field limit where the cavity and extracavity gain formulas coincide. Specifically, as propagation effects become important, the cavity eigenvalue depends in critical ways on the mirror transmission coefficient $T$, which is absent in the extracavity case. It is a nonzero $T$ that causes the internal field to be a function of position and hence to saturate the medium in a nonuniform way. As such the side-mode gain is induced by a spatially varying saturator field determined by the input-field amplitude and the cavity boundary conditions, and can differ significantly from the gains induced by the constant saturator fields assumed in saturation spectroscopy.

As discussed in Ref. 33, inhomogeneous broadening reduces the side-mode gain. References 25 and 26 show that standing waves (e.g., two-mirror cavity) also reduce the effect, and, as shown in the present paper, increased mirror transmissions reduce the instability. This leads us to the conclusion that the most pronounced instabilities occur for the homogeneously broadened, unidirectional ring cavity with low mirror losses. The basic feature characteristic of the other systems is that the primary mode does not saturate all atoms uniformly. Such "averaged" saturation tends to wash out, or at least reduce,

both the size of the hysteresis region and the magnitude of the instabilities.

It is interesting to note that Risken and Nummedal[10] (see also Ref. 11) predicted multimode operation in a homogeneously broadened, unidirectional ring laser by integrating the coupled Maxwell-Bloch equations. For inverted populations in homogeneously broadened media, one might expect single-mode operation to dominate. But for appropriate cavity lengths, population pulsations enter to reduce the mode competition, allowing multimode operation to occur. This phenomenon is closely related to the present instability in optical bistability, and corresponds to mode spacings that yield absorption, rather than gain, in our absorber formulas. For the inverted medium, that absorption turns to gain, which reduces the mode competition.

Let us now return to the mean-field-limit equation (1). Assuming equal decay constants for simplicity, we obtain the self-pulsing instability for $C > 2(1+\sqrt{2})$, as discussed in Sec. III. Since $2(1+\sqrt{2}) > 4$, we see that the instability only occurs when there is a hysteresis cycle. As we have seen in Secs. IV and V, this may not be true when mirror losses become significant. Reference 24 shows that it is no longer true in the case of dispersive OB. This reference also shows that the cavity and extracavity gains differ for dispersive OB even in the mean-field limit.

## ACKNOWLEDGMENTS

We are grateful to R. Bonifacio and F. A. Hopf for stimulating discussions and valuable suggestions. This work was supported in part by the Consiglio Nazionale delle Ricerche (CNR) under Contract No. 78 0091 302, by the Bundesministerium für Forschung und Technologie and Euratom, by the Air Force Office of Scientific Research (A.F.S.C.), the United States Air Force, and in part by the Army Research Office, United States Army.

---

*Deceased.

[1]R. Bonifacio and L. A. Lugiato, Lett. Nuovo Cimento 21, 505 (1978).

[2]R. Bonifacio and L. A. Lugiato, Lett. Nuovo Cimento 21, 510 (1978).

[3]R. Bonifacio, M. Gronchi, and L. A. Lugiato, Opt. Commun. 30, 129 (1979).

[4]R. Bonifacio, L. A. Lugiato, and M. Gronchi, in *Laser Spectroscopy IV, Proceedings of the Fourth Laser Spectroscopy Conference, Rottach-Egern, Federal Republic of Germany, 1979,* edited by H. Walther and K. W. Rothe (Springer, Heidelberg, 1979).

[5]An extensive list of references on optical bistability can be found in Ref. 4 and in H. M. Gibbs, S. L. McCall, and T. N. C. Venkatesen, Opt. News, 1979 (unpublished) (see also their chapter in *Laser Spectroscopy IV*, see Ref. 4).

[6]P. Meystre, Opt. Commun. 26, 277 (1978).

[7]R. Bonifacio and L. A. Lugiato, Opt. Commun. 19, 172 (1976); Lett. Nuovo Cimento 21, 517 (1978).

[8]S. S. Hassan, P. D. Drummond, and D. F. Walls, Opt. Commun. 27, 480 (1978).

[9]R. Bonifacio and L. A. Lugiato, in *Pattern Formation by Dynamic Systems and Pattern Recognition, Proceedings of the International Symposium on Synergetics, Schloss Elmau 1979,* edited by H. Haken (Springer, Berlin, 1979).

[10]H. Risken and K. Nummedal, J. Appl. Phys. 49, 4662 (1968).

[11]R. Graham and H. Haken, Z. Phys. 213, 420 (1968).

[12]S. L. McCall, Appl. Phys. Lett. 32, 284 (1978).

[13]K. Ikeda, Opt. Commun. 30, 257 (1979).

[14]K. Ikeda, H. Daido, and O. Akimoto, Phys. Rev. Lett. 45, 709 (1980).

[15]H. M. Gibbs, F. A. Hopf, D. L. Kaplan, and R. L. Shoemaker, Phys. Rev. Lett. 46, 474 (1981).

[16]V. Benza and L. A. Lugiato, Z. Phys. B35, 383 (1979).

[17]V. Benza, L. A. Lugiato, and P. Meystre, Opt. Commun. 33, 113 (1980).

[18]V. Benza and L. A. Lugiato, in *Proceedings of the International Optical Bistability Conference, Ashville, 1980,* edited by C. R. Bowden, M. Ciften, and H. Robl (Plenum, New York, 1981).

[19]A. Szöke, V. Daneu, S. Goldhar, and N. A. Kurnit, Appl. Phys. Lett. 15, 376 (1969).

[20]R. Roy and M. S. Zubairy, Phys. Rev. A 21, 274 (1980). See Refs. 4, 5, and 18 for more references.

[21]M. Gronchi and L. A. Lugiato, Opt. Lett. 5, 108 (1980).

[22]M. Spencer and W. E. Lamb, Jr., Phys. Rev. A 5, 864 (1972).

[23]R. Bonifacio and L. A. Lugiato, Phys. Rev. A 18, 1129 (1978).

[24]L. A. Lugiato, Opt. Commun. 33, 108 (1980).

[25]F. Casagrande, L. A. Lugiato, and M. L. Asquini, Opt. Commun. 32, 492 (1980).

[26]M. Sargent III, Kvant. Elektron. (Moscow) 10, 2151 (1980) [Sov. J. Quantum Electron. 10, 1247 (1980)].

[27]J. Hambenne and M. Sargent III, Phys. Rev. A 13, 784 (1976); 13, 797 (1976).

[28]L. A. Lugiato, Z. Phys. (in press).

[29]H. Haken, Z. Phys. B21, 105 (1975); 22, 69 (1979).

[30]S. G. Rautian and I. I. Sobel'man, Zh. Eksp. Teor. Fiz. 41, 456, (1961)[Sov. Phys.—JETP 14, 328 (1962)].

[31]B. R. Mollow, Phys. Rev. A 5, 2217 (1972).

[32]S. Haroche and F. Hartmann, Phys. Rev. A 6, 1280 (1972).

[33]S. L. McCall, Phys. Rev. A 9, 1515 (1974).

[34]M. Sargent III and P. E. Toschek, Appl. Phys. 11, 107 (1976).

[35]M. Sargent III, Phys. Rep. 43, 223 (1978).

[36]D. B. Aleksandrov, A. M. Bonch-Bruevich, V. A. Khodovoi, and N. A. Chigir, Zh. Eksp. Teor. Fiz.

Pis'ma Red. 18, 102 (1973) [JETP Lett. 18, 58 (1973)].
[37]F. Y. Wu, S. Ezekiel, M. DuCloy, and B. R. Mollow, Phys. Rev. Lett. 38, 1077 (1977).
[38]See, for example, M. Sargent III, M. O. Scully, and W. E. Lamb, Jr., *Laser Physics* (Addison-Wesley, Reading, Mass., 1974); H. Haken, in *Encyclopedia of Physics*, edited by S. Flugge (Springer, Heidelberg, 1974), Vol. XXV/2c.